CHAPTER II
LITERATURE REVIEW

2.1 Basic Corrosion Principles

2.1.1 Definition of Corrosion

Fontana (1987) defined corrosion as "the destruction or deterioration of a material because of reaction with its environment". It is similarly to the definition from Mattsson (1989) described as "a physicochemical reaction between the material and its environment and leads to changes in the properties of the material". However, some insist that it should be restricted to metals. Corrosion is "the destructive attack of a metal by chemical or electrochemical reaction with its environment" (Uhlig *et al.*, 1991). The corrosion engineers must consider both metals and nonmetals (ceramics, plastics, rubber, and other nonmetallic materials).

Deterioration by physical causes is not called corrosion, but described as erosion, galling, or wear. In some instances, chemical attack accompanies physical deterioration as described by the term: corrosion-erosion, which is defined later as flow-assisted corrosion or flow accelerated corrosion (FAC), corrosive wear, or fretting corrosion (Uhlig *et al.*, 1991).

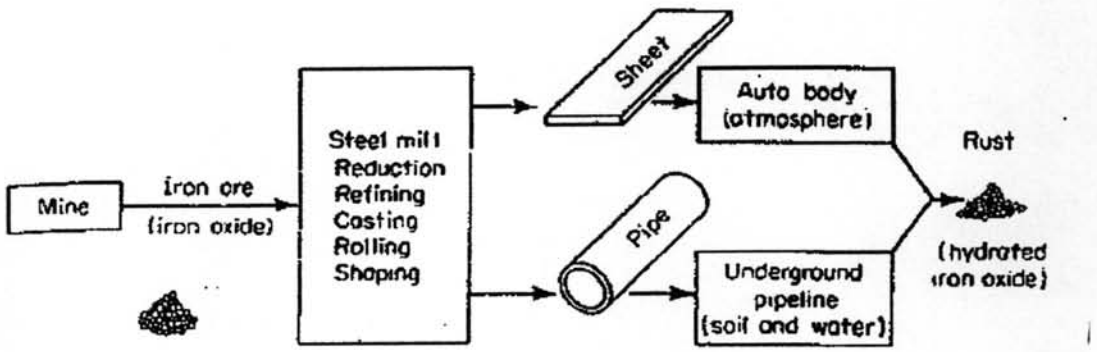

Figure 2.1 Metallurgy in reverse (Fontana, 1987).

Corrosion of metals could be considered as extractive metallurgy in reverse as illustrated in Figure 2.1. Extractive metallurgy is concerned primarily with winning of the metal from the ore and refining or alloying the metal for use. Most iron ores contain oxides of iron, and rusting of steel by water and oxygen results in a hydrated iron oxide. *Rusting* is a term reserved for steel and iron corrosion, although many other metals from their oxides when corrosion occurs (Fontana, 1987).

2.1.2 Classification of Corrosion

Corrosion has been classified in many different ways. It is convenient to classify corrosion by the forms in which demonstrates itself, the basis for this classification being the appearance of the corroded metal. Some of the forms of corrosion are shown in Table 2.1.

Table 2.1 Types of corrosion (Mattsson, 1989)

Type of Corrosion	Description
Uniform corrosion	Characterized by corrosive attack proceeding evenly over the entire surface area, or a large fraction of the total area. General thinning takes place until failure. On the basis of tonnage wasted, this is the most important form of corrosion
Pitting corrosion	A localized form of corrosion by which cavities or "holes" are produced in the material. Pitting is considered to be more dangerous than uniform corrosion damage because it is more difficult to detect, predict and design against
Crevice corrosion	A localized form of corrosion usually associated with a stagnant solution on the micro-environmental level. Such stagnant microenvironments tend to occur in crevices (shielded areas) such as those formed under gaskets, washers, insulation material, fastener heads, surface deposits, is banded coatings, threads, lap joints and clamps

Table 2.1 Types of corrosion (cont'd)

Type of Corrosion	Description
Galvanic corrosion	Corrosion damage induced when two dissimilar materials are coupled in a corrosive electrolyte
Erosion corrosion	Acceleration in the rate of corrosion attack in metal due to the relative motion of a corrosive fluid and a metal surface. The increased turbulence caused by pitting on the internal surfaces of a tube can result in rapidly increasing erosion rates and eventually a leak
Cavitation	Occurs when a fluid's operational pressure drops below it is vapor pressure causing gas pockets and bubbles to form and collapse. This can occur in what can be a rather explosive and dramatic fashion
Fretting corrosion	Rrefers to corrosion damage at the asperities of contact surfaces. This damage is induced under load and in the presence of repeated relative surface motion, as induced for example by vibration
Intergranular Corrosion	The microstructure of metals and alloys is made up of grains, separated by grain boundaries. Intergranular corrosion is localized attack along the grain boundaries, or immediately adjacent to grain boundaries, while the bulk of the grains remain largely unaffected
Exfoliation Corrosion	Corrosion products building up along these grain boundaries exert pressure between the grains and the end result is a lifting or leafing effect.
Dealloying or selective leaching	The selective removal of one element from an alloy by corrosion processes.
Stress corrosion cracking (SCC)	The cracking induced from the combined influence of tensile stress and a corrosive environment

2.1.3 Corrosion Rate Expressions

If a thermodynamic driving force exists for a corrosion process, then it will take place. The rate of corrosion must be expressed quantitatively in order to compare its corrosion resistance with other processes. The rate of corrosion can vary within wide limits. In certain case it can be large and cause serious damage to the material. In other cases it can be small and of little practical importance; this is a result of inhibition of one or more of the electrode reactions.

Corrosion rates have been expressed in a variety of ways in the literature: such as the change in weight of the material, the depth of the surface zone which has been corroded away, the number and quantity of pits formed, the amount of corrosion products, changes in the ultimate strength, yield strength or rupture strain of the metal, etc. The change in the magnitude of these per unit of time is a measure of the corrosion rate. Another measure is expressed in term of the density of the corrosion current. In Table 2.2 Some of the most frequently encountered units of corrosion rate are given (Mattsson, 1989).

Table 2.2 Various units for corrosion rates (Mattsson, 1989)

Corrosion effect	**Unit**
Weight change	g/m^2 year mg/dm2 day = mdd
Increase in corrosion depth	μm/year mm/year = 10^3 μm/year inch per year = ipy = 25.4 mm/year mil per year = mpy = 10^{-3} ipy = 25.4 μm/year
Decrease in ultimate strength, yield strength or rupture strain	percent/year (of initial value)
Corrosion current	mA/cm^2

A good corrosion rate expression should involve (1) familiar units, (2) easy calculation with minimum opportunity for error, (3) ready conversion to life in year, (4) penetration, and (5) whole numbers without cumbersome decimals. From an

engineering viewpoint, the rate of penetration, or the thinning of a structure piece, can be used to predict the life of a given component (Fontana, 1987).

Fontana began promoting the expression *mils per year*, or milli-inch per year, in 1945, and it is now widely used. This expression is readily calculated from the weight loss of the metal specimen during the corrosion test. The formula for calculating this rate is

$$\text{Mils per year (mpy)} = \frac{534W}{DAT} \tag{2.1}$$

where W = weight loss, mg

D = density of specimen, g/cm^3

A = area of specimen, sq. in.

T = exposure time, hr

Mils per year is the most commonly used corrosion rate expression in the United States. It is popular because it expresses corrosion rate in terms of penetration using small integers. However, a substitute expression is required to facilitate the conversion to the metric system. Some equivalent metric penetration rates are:

$$1 \text{ mpy} = 0.0254\frac{\text{mm}}{\text{year}} = 25.4\frac{\mu\text{m}}{\text{year}} = 2.90\frac{\text{nm}}{\text{hr}} = 0.805\frac{\text{pm}}{\text{sec}} \tag{2.2}$$

Before a substitute metric corrosion rate expression is selected, it is important to consider how metric measurements are used to describe dimensions. Although nm/hr and especially pm/sec provide conveniently small whole numbers, they required additional conversion before they can be related to the typical dimensions of engineering structures. Micrometers/yr (μm/yr) and mm/yr are the most useful expressions in metric system; the former for low corrosion rates and the latter for rapid rates.

The above two expressions are easily calculated from weight-loss data by equations, Eqn. (2.1) and (2.2), similar to that described in mpy unit.

$$\text{Mils per year (mpy)} = \frac{534W}{DAT} \tag{2.3}$$

where W = weight loss, mg

D = density of specimen, g/cm^3

A = area of specimen, cm^2

T = exposure time, hr

Increasingly, corrosion rates determined by electrochemical techniques are expressed in terms of current density. These expressions can be converted into penetration rates by the following expression based on *Faraday's law*:

$$\text{Corrosion penetraion rate} = K\frac{ai}{nD} \tag{2.4}$$

where a = atomic weight of metal

i = current density, $\mu a/cm^2$

n = number of electron lost (valence change)

(This parameter is determined by analysis of the solution or by measuring the potential and pH and referring to appropriate thermodynamic data, potential-pH diagrams.)

D = density, g/cm^3

K = constant depending on the penetration desired

(For mpy, μm/yr, and mm/yr, the values of K are 0.129, 3.27, and 0.00327, respectively.)

2.1.4 Physical Methods for Corrosion Investigation

According to Mattsson (1989), Corrosion investigations are carried out in many contexts, e.g. for:

- the development of new materials and corrosion-preventing agents,
- the selection of construction materials,
- the quality control of materials and protective agents,
- corrosion monitoring and analysis of corrosion failures.

There are several methods to investigate corrosions depending on the purpose of the determination, for example for corrosion testing, corrosion monitoring, electrochemical investigation, and physical investigations. The conventional methods for chemical analysis, metallographic investigations, and tensile testing and special methods are used for exposure testing and corrosion monitoring as well as for electrochemical and physical surface investigations.

For the physical surface investigations corrosion usually leads to changes in the surface condition of a material, e.g. corrosion attack, or the production of a coating of corrosion products or a passive layer. A number of physical methods are available for the investigations of these changes, e.g. metallographic microscopy, electron microscopy, X-ray or electron diffraction as well as surface physical methods. In Table 2.4, a selection of such methods and their possibilities and limitations is described.

Table 2.3 Some physical methods used in corrosion investigation (Mattsson, 1989)

Type	Principle employed	Remarks
Optical microscopy	The surface of the sample is examined under a microscope illuminated with visible light.	Magnification: 10 – 1000X
Scanning electron microscopy (SEM)	A view of the sample surface is obtained with the aid of a reflected electron beam. X-rays emitted make chemical analysis possible by so-called energy-dispersive X-ray spectroscopy (EDS). The method requires a vacuum.	Magnification: $10^2 - 10^4$X
Transmission electron microscopy (TEM)	An electron beam is allowed to pass through a thin sample ($\leq$1 μm) and gives an image of the sample on a fluorescent screen. The diffraction pattern of the radiation makes phase identification possible. The method required a vacuum.	
Ellipsometry	The sample surface is irradiated with polarized light which is reflected. Change in the direction of polarization is a measure of the thickness of the surface coating. The method can be applied to samples in liquids.	Can be used for coating thickness $\geq$0.1 nm

Table 2.3 Some physical methods used in corrosion investigation (Mattsson, 1989) (cont'd)

Type	Principle employed	Remarks
X-ray diffraction	A monochromic X-ray beam is passed through the sample. The diffraction pattern makes phase identification possible.	Can be used on samples of thickness 10 – 100 μm
X-ray fluorescence	The sample surface is irradiated with a high-energy X-ray beam. X-ray radiation emitted makes chemical analysis of surface zone possible.	Detection limits: 10 – 100 ppm for elements with atomic numbers above 4
Microprobe	The sample surface is irradiated with a high-energy X-ray beam. X-ray radiation emitted makes chemical analysis of surface possible.	Detection limits: 10 – 150 ppm for elements with atomic numbers above 10
ESCA or X-ray induced photo-electron spectroscopy (XPS)	The sample surface is irradiated with X-rays. Emission of photo- electrons makes possible analysis of elements in the surface zone and their valence state. The method requires a vacuum.	- The analysis is representative for a surface zone of 1 – 3 nm. - Detection limits: *ca.* 0.1% for elements with atomic numbers above 1
Auger electron spectroscopy	The sample surface is irradiated with electrons. Emission of so-called Auger electrons makes chemical analysis of surface zone possible. Via ion etching the variation in depth can be determined. The method requires a vacuum.	- The analysis is representative for a surface zone of 0.5 – 3 nm. - Detection limits: *ca.* 0.1% for elements with atomic numbers above 2

Table 2.3 Some physical methods used in corrosion investigation (Mattsson, 1989) (cont'd)

Type	Principle employed	Remarks
Surface-enhanced Raman spectroscopy	The sample surface is irradiated with a beam of monochromic light. The reflected light contains a Raman spectrum with makes possible the identification of ions and bonds in thin coatings, especially on Au, Ag and Cu. The method can be used for samples in aqueous media.	Can be used in the study of thin coatings (≤10 nm)
Ion microprobe analysis (SIMS)	The sample surface is irradiated with a beam of ions. Freed molecules are analyzed in a mass spectrometer. A depth profile is automatically obtained due to the sputtering effect of the ion beam.	- Detection limit in the ppb/ppm region - Applicable for all elements

2.2 CANDU Nuclear Reactor

Although nuclear reactors are complex, the basic principles underlying their operation can be understood relatively easily. A nuclear chain reaction is used to produce heat. The heat turns a fluid to steam and this steam is used to turn turbines and generate electricity. The CANDU is one type of nuclear reactor. CANDU stands for CANada Deuterium Uranium, indicating the use of deuterium (D_2O), or heavy water, for the moderator and coolant and natural uranium (UO_2) for the fuel.

A schematic of the CANDU nuclear reactor illustrating these features is shown in Figure 2.2. Pressure tubes containing fuel bundles pass horizontally through a vessel called calandria containing heavy-water moderator. A nuclear reaction, fission reaction, in the fuel bundles heats the heavy-water coolant. This heat is carried to the steam generator where it is transferred to ordinary water in a separate circuit to produce steam.

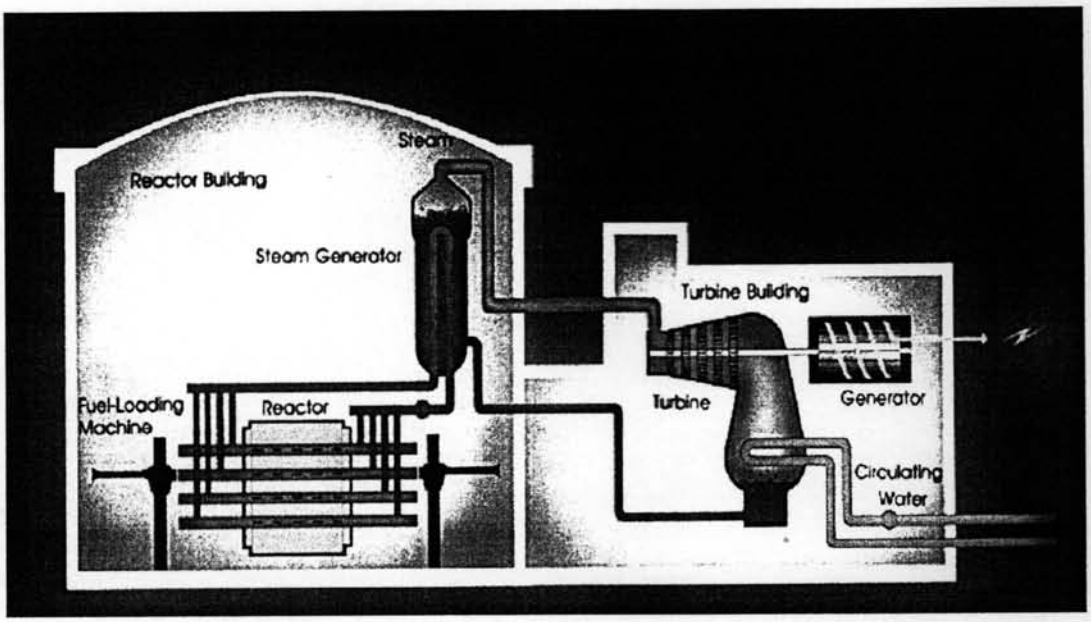

Figure 2.2 Schematic of a CANDU nuclear reactor. (Tammemagi *et al.*, 2002)

The steam is sent through turbine, which turns a generator to produce electricity. Circulating water from outside condenses the steam to water, which is then cycled back to the steam generator. The figure also shows the fueling machine and the reactor containing building (Tammemagi *et al.*, 2002).

There are two coolant loops in a CANDU reactor, the primary coolant loop and the secondary coolant loop, which are the system for carrying generated heat from the fission reaction. The primary coolant, the heavy water, carries heat from the reactor core to the steam generator where the secondary coolant, which is the light water (H_2O), is converted into the saturated steam by the recovered heat from the primary coolant.

The CANDU primary coolant loop consists of three major components: the reactor core, the steam generator and the piping system as shown in Figure 2.3. The reactor core is a horizontal cylindrical tank (calandria) containing the heavy water water (D_2O) moderator which is maintained at 60°C. The reactor core consists of 380 fuel channels, 190 inlet feeders and 190 outlet feeders, holding Zr-2.5%Nb pressure tubes. Each pressure tube containing twelve Zircaloy-4 fuel bundles fuelled with natural UO_2 and sheathed with Zircaloy-4. The pressure tubes are connected to the

feeders and headers via end fittings made of 400-series stainless steel while a Grayloc connector attaches each feeder to its fuel channel end-fitting.

The feeder, made of SA-106 Grade B carbon steel, carry the coolant directly into and out of the reactor fuel channels – the "inlet" and "outlet" feeders respectively. In a CANDU-6 reactor, two sizes of piping are employed for outlet feeders close to reactor face – nominally 2 inch and 2.5 inch (actually 6.03 cm and 7.30 cm outside diameter respectively). Also, the steam generators are tubed with Alloy-800 – in the CANDU-6 reactor.

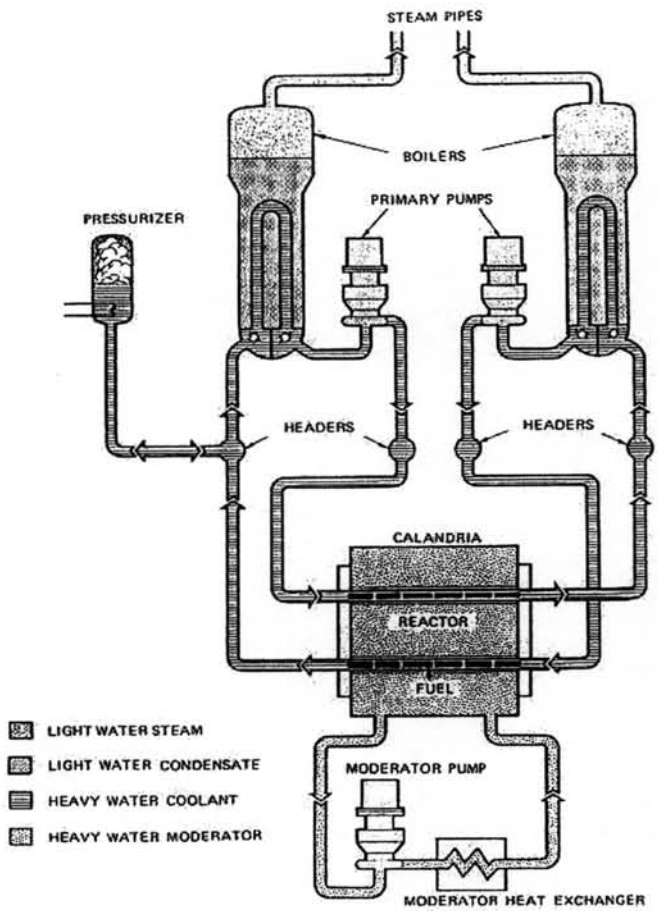

Figure 2.3 Schematic of the primary coolant system of CANDU reactor (Silpsikul, 2001).

The primary coolant D_2O enters the core at 265°C and leaves at 310°C, with steam qualities ranging up to 6%. The steam survives through the outlet feeders and headers to the steam generators, and quality actually increases slightly in transit because of the pressure drop along the piping. Average linear velocities of the coolant in the outlet feeders ranges from 8 m/s to about 16 m/s. The constant chemical conditions are maintained, with dissolved D_2 within the specification of 3 to 10 cm^3/kg (at STP). The alkalinity of the coolant is adjusted with ion-exchange in the purification system and with added lithium hydroxide to within the range of pH 10.3 to 10.8 at room temperature (Lister *et al.*, 1998).

The summary of material construction of each component is shown in the following table, Table 2.4.

Table 2.4 Material construction of components in CANDU primary coolant loop (Taenumtrakul, 2005)

Component	Material
Reactor core	Zirconium alloy 2.5%Nb
Steam generator*	Nickel alloy - Monel 400 - Inconel 600 - Incoloy 800
Piping	A-106 Grade B Carbon Steel

*Depends upon the CANDU model

2.3 Corrosion of Feeder Pipes at Nuclear Generating Station

2.3.1 The Discovery of the excessive wall thinning of CANDU feeders

Lister *et al.* (1998) stated that the feeder wall thickness from the routine survey measurement, which have been carried out on inlet and outlet feeders at all CANDU reactors by using ultrasonic techniques since their start up, have shown no untoward corrosion. These measurements are usually made close to the

reactor inlet and outlet headers at places that are reasonably accessible. However, it became clear that excessive thinning of the first few meters of the outlet feeders was widespread after measurements were made at Point Lepreau during an extended outage in 1995 – 1996 at places close to the reactor face.

Subsequently measurement at other reactors confirmed that CANDUs generally are experiencing such thinning at rates far in excess of what was predicted from early measurements in autoclaves or out-reactor loops or even from more recent theoretical modelling. Actually, some feeders were estimated to have thinning rates greater than 150 μm/year by intensive monitoring campaigns and from the best estimates of starting thicknesses. In contrast, it should be noted that from laboratory testing under conditions similar to those of CANDU coolant the accepted values for carbon steel corrosion rate obtained were generally below 10 μm/year. Corrosion rates measuring on inlet feeders were indicated in the neighborhood of this value.

The CANDU-6s such as the Point Lepreau and Gentilly-2 reactors are the most seriously affected, for they are experiencing the highest thinning rates and have been operating the longest. Without remedial action, they may not last their design lifetime unless some feeders are replaced.

2.3.2 Observations at Point Lepreau Generating Station (PLGS)

The Point Lepreau CANDU in New Brunswick has been at the forefront of the reactor studies and has now accumulated a considerable amount of information. The measurement of the wall thickness of the Point Lapreau feeders was done by staffs of the New Brunswick Research and Productivity Council (RPC), who use an ultrasonic technique with a reputed accuracy of +/- 10 μm (Lister *et al.*, 1997). In the field, accuracies in the order of +/- 100 μm are probably obtained.

The first and second bends of feeders were the places where most of measurements were made, for it is there that the maximum thinning rate has been anticipated – because of the high turbulence of the coolant leaving the fuel channel – and it is there that the wall thickness was initially the lowest – because of the pipe bending which thins the metal at the outside of the bend, i.e., at the extrados. The

piping for these lower outlet feeders is either 2 inches nominal outside diameter (in 60 channels) or 2.5 inches (in 320 channels).

As demonstrated in Figure 2.4, the feeder arrangement in this area is congested, making it difficult on many channels to apply the ultrasonic detector in a full circumferential scan to any distance away from the Grayloc. Furthermore, radiation fields at the reactor face and towards the header tend to be quite high, obstructing the monitoring even more.

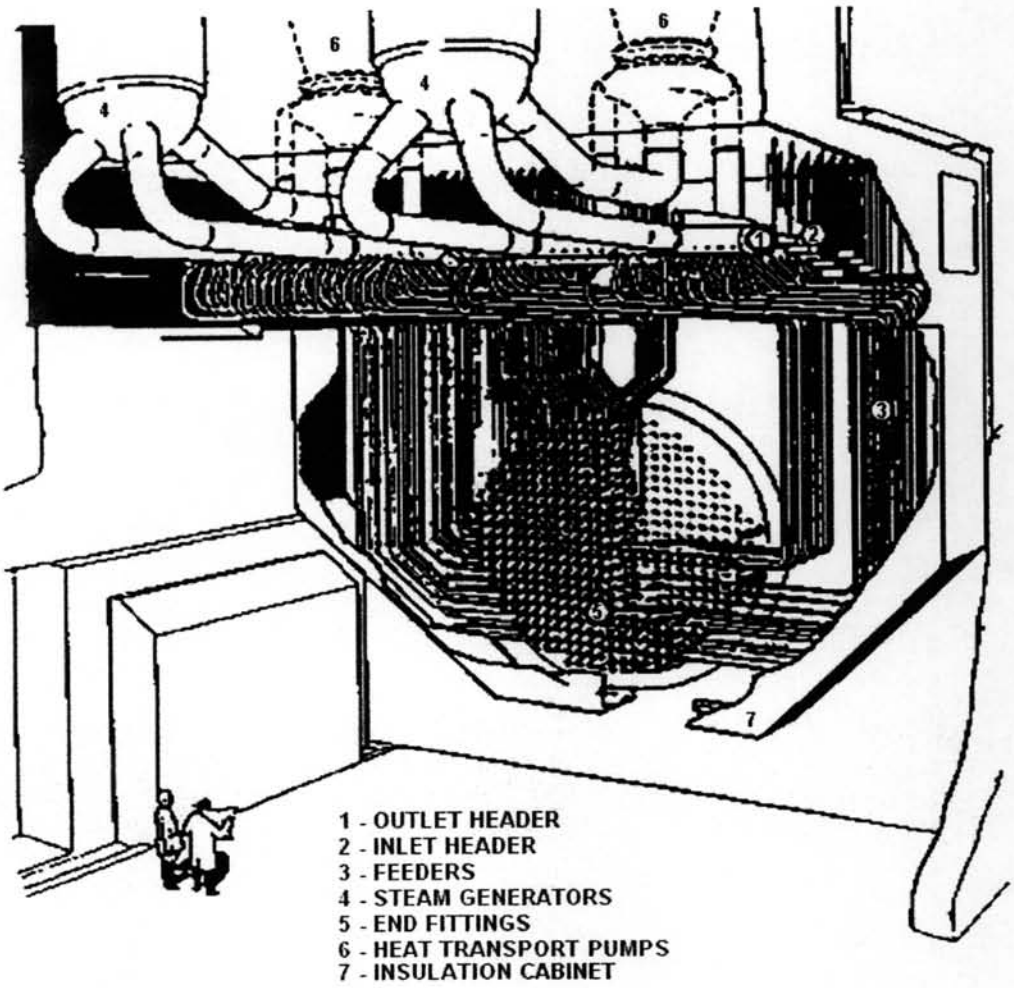

Figure 2.4 Arrangement of feeders and headers (Lister *et al.*, 1997).

In spite of the difficulties, many measurements were made at PLGS in 1996. About 7,000 determinations of wall thickness were made on 64 outlet and 3 inlet feeders. In addition, early in 1997 a heavy-water leak was traced to outlet feeder

SO8, which had developed a crack at the first bend after the Grayloc and the replacement of about a meter of the pipe has provided a length of thinned feeder for detailed examination. And finally, one outlet feeder (F11) was monitored up o 3 meters or so downstream of the Grayloc. This provided information on the thinning rate beyond the first bends, including some straight sections.

The major findings to date of the PLGS measurement program are as follows (Lister *et al.*, 1997):

1. Outlet feeders were corroding much more rapidly than inlets. All of the three inlet feeders that were measured indicated corrosion rates averaged over the lifetime of the plant below 20 μm/year. In contrast, the outlets indicated rates up to 150 μm/year.

2. Steam quality did not seem to affect thinning rate. Over the range of average steam qualities below 4%, no consistent effect on thinning rate had been detected.

3. The circumferential variation in thinning rate at the bends was between about 15% and 80%, with maximum generally close to the bend extrados.

4. The axial variation in thinning rate over the first 3 meters or so was less than about 20%. This observation, along with the previous two, was somewhat surprising given that the thinning phenomenon was expected to be sensitive to fluid turbulence effects, which should be much more severe at the bend extrados and be markedly affected by steam quality.

5. Thinning rates were strongly correlated with coolant velocity. For example, the values measured at the first bend extrados for both 2 inches and 2.5 inches feeders together indicate a correlation with linear velocity raised to power 1.52, though the data were quite scattered (Figure 2.5).

6. At positions away from the reactor face (i.e., close to the outlet header where the routine survey measurements have been made) thinning rates were low. It explained why the excessive thinning was not detected earlier, but raised the question why the thinning should decline only after 3 meters beyond the outlet Grayloc, which was the distance scanned on F11. Certainly, some of the feeders

measured at the header were of larger diameter there than closer to the reator, so they would contain coolant of lower velocity.

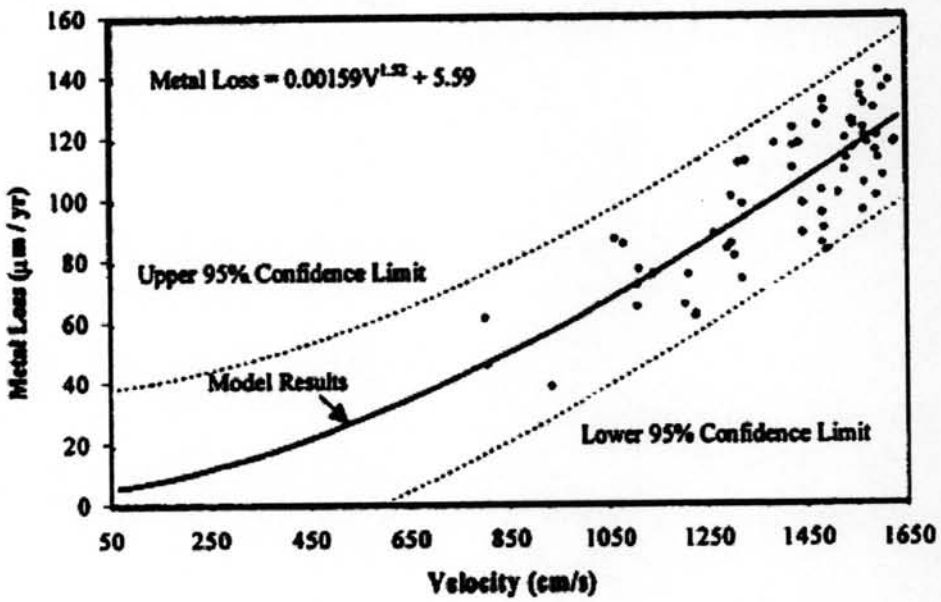

Figure 2.5 Feeder thinning rate (metal loss rate) at extrados of first bend on 2 inches and 2.5 inches feeders at Point Lepreau (Beshara, 1997).

7. The chromium content of the steel was important. The piping is made of carbon steel – designated ASTM A106-B – and this material has an upper limit on chromium content of 0.40%. The specification for the PLGS feeders, however, was made with a view of minimizing activity transport, so low-cobalt material was procured. This necessarily minimized the chromium content, too, leading to concentrations of 0.02% - 0.03% Cr. Also, analysis of the removed section of pipe indicated that SO8 had a chromium content of 0.02%. The Grayloc hub, however, contained 0.13% Cr, and the weld joining the hub to the pipe contained an intermediate concentration of 0.07%. Detailed examination of sections through the hub-feeder weld of SO8 showed that the thinning was minor for the Grayloc, and increased stepwise to the pipe. This was a strong indication that chromium content was important parameter in the thinning phenomenon, and that the specification of

chromium content at the upper end of the permitted range for A106-B for future CANDU feeders should mitigate the thinning problem.

8. The accelerated thinning led to a "scalloped" or "dimpled" surface with only a thin oxide layer. Such surface scalloping was typical of the attack by flow-accelerated (assisted) corrosion or FAC of carbon steel in feed water systems or even of the sculpting of clay, mud or rock-river beds by fast-flowing streams.

2.4 Flow-Accelerated Corrosion (FAC) in CANDU Feeders

Fontana (1987) defined flow-accelerated corrosion (FAC) or sometimes called erosion-corrosion as the acceleration or increase in rate of deterioration or attack on a metal because of relative movement between a corrosive fluid and the metal surface. Generally this movement is quite rapid, and mechanical wear effects or abrasion are involved. Metal is removed from the surface as dissolved ions, or it forms solid corrosion products that are mechanically swept from the metal surface. Sometimes movement of the environment decreases corrosion, but this is not FAC because deterioration is not increased.

For the CANDU feeder pipes, it has been found that the corrosion is not only uniform corrosion but also susceptible to erosion, and therefore attributed to FAC. FAC is a significant problem with carbon steel components which handle rapidly moving water or water/steam mixtures in the power generation industry (Villien *et al.*, 2001).

Villien *et al.* (2001) stated that the symptomatic of the attack by FAC of carbon steel in boiler feed-water systems is "surface scalloping". Scallops were also observed in the primary coolant system of CANDU reactors as shown in Figure 2.6. It can be seen that the formation and the evolution of scallops in outlet feeders made of carbon steel play a major role on the thinning rate of the pipes, which is proceeding much faster than expected

An oxide film formed on the carbon steel surface and protected the surface by limiting the diffusion processes that control corrosion were the main assumption in FAC. Corrosion is increased if erosion and/or dissolution make the film thinner. The oxide film formation at the metal surface equals its dissolution at the oxide-

coolant interface, at steady state. The increasing in the fluid velocity can increase the flux of removed oxide to the bulk coolant. Also, at bends or elbows, the turbulence is very high and these places are expected to be particularly sensitive.

Figure 2.6 Scalloping on the inner surface of a carbon steel feeder pipe (Villien *et al.*, 2001).

The FAC in outlet feeders of a power plant can be described as a combination of dissolution-controlled and erosion-controlled corrosion. Dissolution and mass transport may act together and involve convective diffusion, while the erosion component is characterized by the combined action of flow-induced mechanical forces (shear stresses, pressure variation by high flow velocity and particle impact in multiphase flows) and electrochemical processes (Villien *et al.*, 2001).

2.5 Mechanism of the Oxide Film Growth

The nature and properties of the protective films that forms on some metals or alloys are important from the standpoint of resistance to erosion corrosion or FAC. The ability of these films to protect the metal depends on the rate or ease with which they form when originally exposed to the environment, their resistance to mechanical damage or wear, and their rate of re-forming when destroyed or damaged. A hard,

dense, adherent, and continuous film would provide better protection than one that is easily removed by mechanical means or shear due to flow. A brittle film that cracks or spalls under stress may not be protective. Sometime the nature of the protective film that forms on a given metal depends upon the specific environment to which it is exposed, and this determines its resistance to erosion corrosion by that fluid (Fontana, 1987).

Under alkaline, reducing conditions in high-temperature water, carbon steel develops a film of magnetite. As observed in experiments in closed and static systems, such as autoclaves, and boilers, the film is typically double-layered with the Potter-Mann structure. The inner-layer magnetite, adjacent to the metal, is fine-grained and grows at the metal-oxide (M-O) interface. The outer layer magnetite is precipitated from solution at the oxide-coolant (O-C) interface and is composed of crystallites, generally octahedral in shape, of a few μm in thickness (Lang *et al.*, 2002).

A considerable number of investigations have been devoted to the study of the formation mechanism of a passive film. The corrosion of carbon steel and low alloy steel, in the absence of oxygen, involves the inward diffusion of oxygen bearing species to the metal/oxide interface and the outward diffusion of the iron ions to the solution. The solution becomes saturated with dissolved iron when iron ions pass into it, resulting in the formation of the outer oxide layer by precipitation and growth on the inner oxide layer.

The generated speies in the system can diffuse through the existence oxide layer in high temperature by the short circuit routes such as micro-pores and grain boundaries, rather than the lattice. Therefore, in the absence oxygen as in the primary system of CANDU reactors, the possible oxygen bearing species might be either water molecules, oxygen ions or hydroxide ions diffusing along the short circuit routes.

Cheng and Steward (2004) stated that water should be the main oxygen bearing species involving the formation of the magnetite film and also acts as a binder between oxide chains because oxygen ions will involve the formation of the oxide film only after a sufficiently anodic potential is applied and a de-protonation of water takes place. Hydroxide ions are not likely to be the diffused species due to the

electrical charge strength across the thin film thickness which is high resulting in the blocking of negative species, the hydroxide ion, which moves toward to the metal surface.

Hydrogen ions formed diffuse inward through the oxide film to neutralize the electron from anodic reactions and form as H_2 at the metal/oxide interface. Diffusion of hydrogen ions through the oxide film is driven by the concentration and electric potential gradient. It is expected that hydrogen ions diffuse through the oxide film relatively slowly because the ionic crystalline oxide has a low hydrogen diffusion coefficient and thus, provides a definite resistance to hydrogen resistance. However, Tomlinson (1981) proposed that the diffusion of hydrogen ions through the lattice should take place without physical hindrance because the size of the hydrogen ions is very small ($\sim 10^5$ times smaller than other ions), similar in size to electron.

The iron ions generated by the anodic dissolution reaction of steel are immediately formed as an inner oxide layer at the metal/oxide interface. The remaining of the dissolved iron diffuses outward through the oxide layer and forms an outer oxide layer at the oxide /solution interface. The schematic diagram of the magnetite film formed on a steel surface in high temperature water is shown in the Figure 2.7.

At the steel/oxide interface, iron dissolves into the solution when no oxide layer exists. Water molecules diffuse through the inner oxide layer and directly react with the metal surface resulting in the formation of the magnetite film or as inner oxide layer. Hydrogen ions from the water solution can also diffuse inward through the oxide layer under the concentration and potential gradient and form hydrogen atoms at the steel/oxide interface. Tomlinson (1981) reported that up to 90% of the hydrogen atoms form at the steel/oxide interface and more than 99 % probably diffuse through the metal at the temperature of interest.

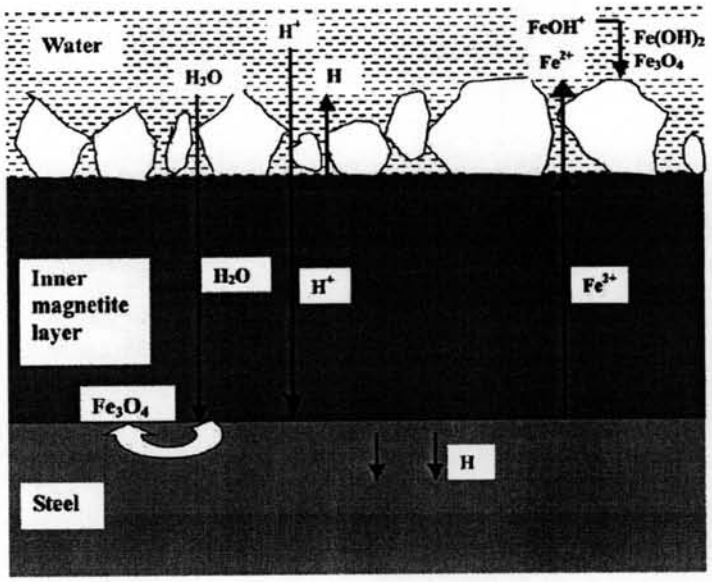

Figure 2.7 Schematic view of the formation mechanism of magnetite on the steel surface in high temperature water (Cheng and Steward, 2004).

At the oxide/solution interface, The remainder of the iron ions diffuse through the inner oxide layer as $Fe(OH)^+$. For high temperature water, $Fe(OH)^+$ will change to FeO, on unstable species, and finally, react with water to form an outer oxide layer. Robertson (1989) and Lang (2000) stated that the outer layer can dissolve in the fluid, depending on the water chemistry. At the same time, hydrogen ions can also be produced by the Schikorr reaction and diffuse through the inner oxide layer.

2.6 Characterization of Oxide Film on Feeder Pipe Steels

The operating conditions of the primary system have an important effect on the magnetite layer formed on the feeder pipe surface. An increase in magnetite solubility with temperature (at pH of 10, at room temperature, or above) leads to under-saturation of the coolant at the reactor outlet. This causes magnetite dissolution into the bulk coolant (Silpsrikul, 2001).

The composition of the steel is important in feeder pipe FAC. The Chromium (Cr) content of the steel affects the properties of the oxide film as shown in Figure 2.8. Steel containing higher Cr has a smaller particle size and higher packing density. This provided a finer grain size and more compact oxide layer. The more compact oxide layer enhanced the corrosion resistance by controlling the dissolution of iron (Fe), (Taenumtrakul, 2005).

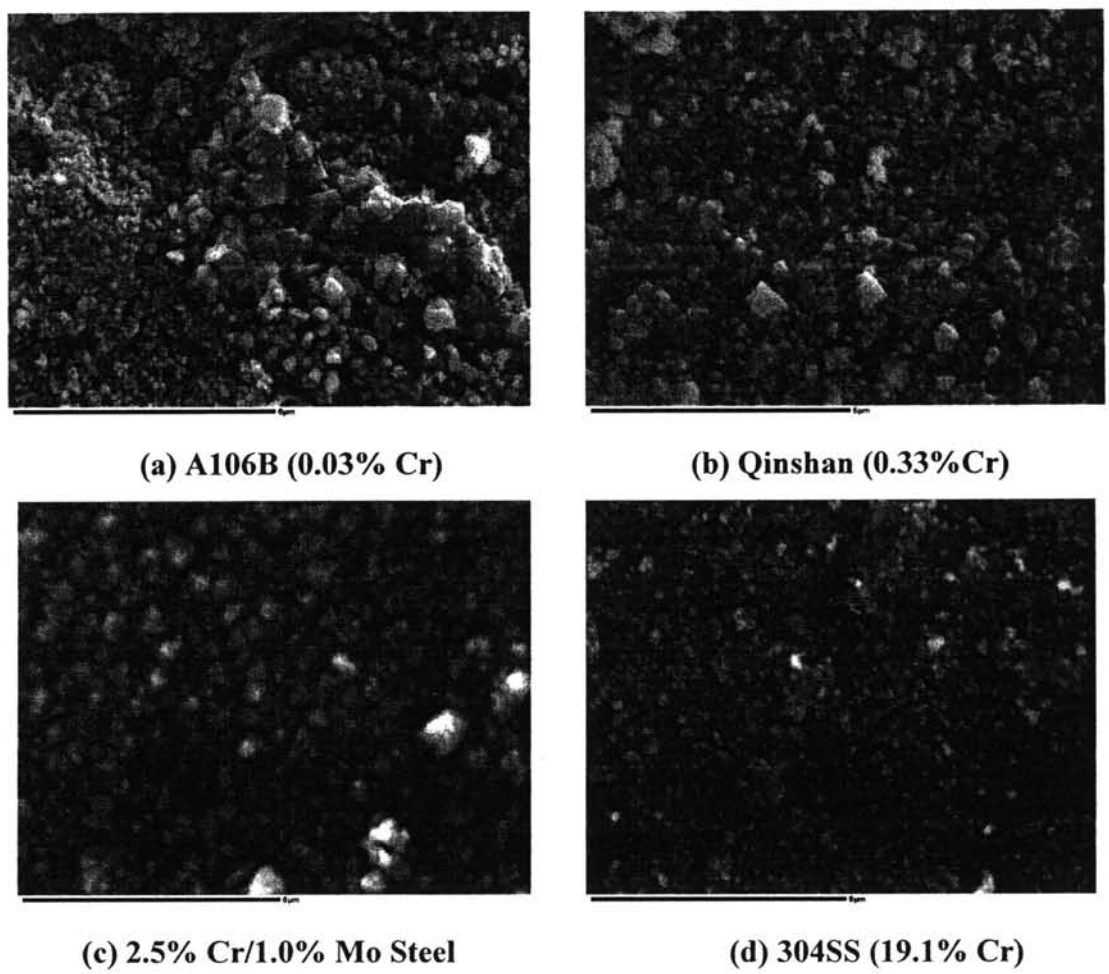

(a) A106B (0.03% Cr) **(b) Qinshan (0.33%Cr)**

(c) 2.5% Cr/1.0% Mo Steel **(d) 304SS (19.1% Cr)**

Figure 2.8 SEM surface micrographs of oxide film formed on different steels at 10,000X magnification (Taenumtrakul, 2005).

As mentioned above, the velocity of the coolant is an important parameter in FAC. The velocity of the coolant in the pipe produces shear stress at the surface. Consequently, erosion of the magnetite can occur. Suthicharoen (2006) investigated

this effect on the surface properties of the oxide film as shown in Figure 2.9. The result showed that the oxide formed consisted of two layers, an inner layer with fine oxide grains and an outer layer of large oxide crystals. This type of oxide film was not found in previous experiments. The coolant velocity did not effect the oxide composition, but did effect the outer oxide morphology. There was a fluffy layer of fine particles which cover the outer oxide layer formed under the high coolant velocity. A high coolant velocity resulted in a thin oxide layer and a higher corrosion rate, presumably due to high shear stress at the wall.

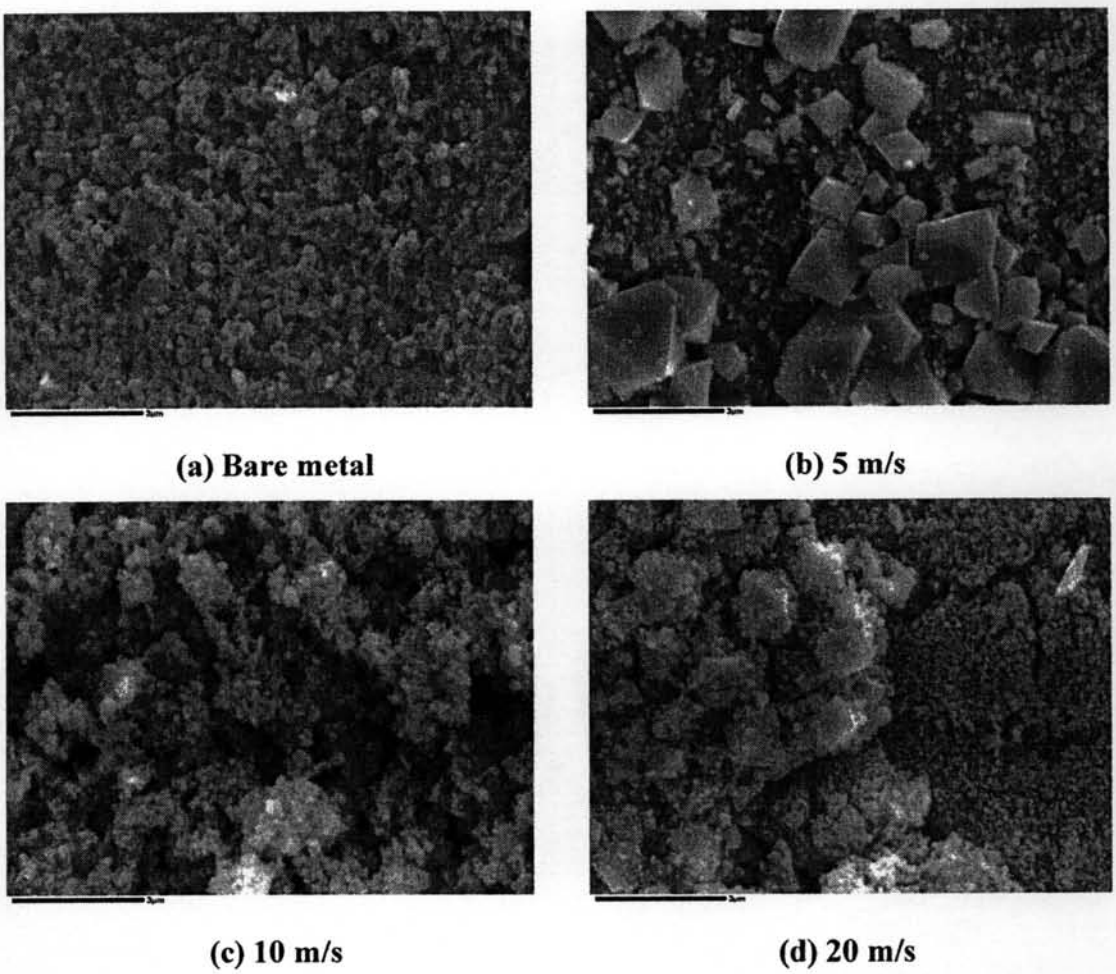

(a) Bare metal **(b) 5 m/s**

(c) 10 m/s **(d) 20 m/s**

Figure 2.9 SEM surface micrographs of oxide film formed under different coolant velocities at 10,000X magnification (Suthicharoen, 2006).

2.7 The Possible Inhibition of Feeder Thinning by Titanium Dosing

Some recent work has focused on using coolant additives to mitigate FAC. Bateman *et al.* (2002) mentioned that from the early work at University of New Brunswick (UNB) had shown that titanium might be a possible candidates as an additive that could reduce the FAC rate by altering the oxide layer on the outlet feeders.

The impact on a carbon steel plug whose thickness was being monitored by an ultrasonic technique was first occurred in an experiment under a high-velocity jet of simulated primary system coolant. After insertion of plug in a loop that had a significant portion of titanium as its construction material – autoclaves and tubing, it was found that the removed samples had a thick surface oxide with a large titanium constituent, which was determined to be ilmenite ($FeTiO_3$). Also, it was apparent that an ilmenite film deposited on the carbon steel surface was adherent and protective since it could withstand a jet impact of 20 m/s. The result showed that the reduction in corrosion rate was found to be 69% after the titanium injection.

A complementary study by Bateman *et al.* (2002) was also determined the solubility of titanium oxides. Two methods were used to determine the solubility of titanium oxide – calculation of the theoretical solubility using standard thermodynamic relations and direct measurement using a high- temperature autoclave loop. The measured solubility at different pH values and temperature of rutile and ilmenite are illustrated in Figures 2.9 and 2.10, respectively.

Bateman *et al.* (2002) also concluded about the solubility of titanium that titanium dioxide, in rutite form, had a measurable solubility within the range of 0.1 to 0.3 μg/kg in simulated CANDU primary coolant system while the value obtained from ilmenite form was expected to be higher due to its higher Gibbs free energy.

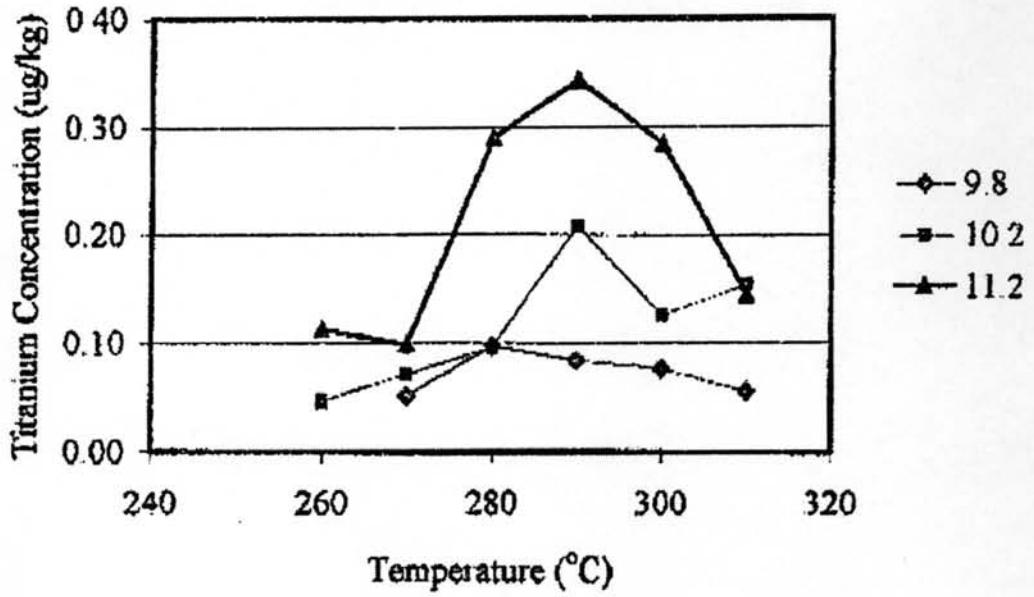

Figure 2.10 Measured solubility of titanium from rutite (Bateman *et al.*, 2002).

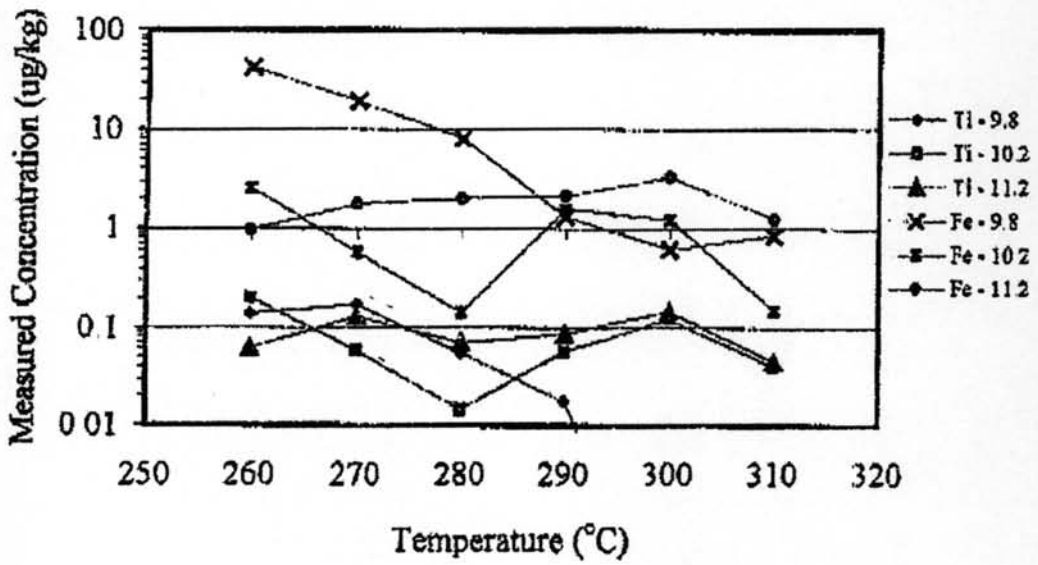

Figure 2.11 Measured solubility of iron and titanium from ilmenite (Bateman *et al.*, 2002).

2.8 Modelling of FAC in CANDU Reactors

In order to predict the FAC phenomenon, it is necessary to develop a model. Such a model can be used to predict the thinning rates of various outlet feeder pipes within the reactor. The model can also be used to interpret data from the laboratory tests, (Silpsrikul, 2001). A model of the FAC process that incorporates magnetite formation by corrosion, oxide film dissolution and mechanical removal by erosion has been developed, (Lister *et al.*, 1994).

Traditional descriptions of FAC have considered mass transport factors in the development of the magnetite corrosion product film, which controls the corrosion of the underlying carbon steel, (Lister *et al.*, 2001).

As shown in Figure 2.11, the corroding metal deposits a fine-grained, inner layer of magnetite at the metal-oxide (M-O) interface. Approximately half of the corrosion product diffuses as ferrous ions through this layer into the fluid boundary layer, (Lister *et al.*, 2001). Under normal circumstances, in coolant already saturated in dissolved iron, this diffusing material promotes precipitation of an outer layer of magnetite in the form of octahedral crystallites. In coolant under-saturated in dissolved iron, the outer layer will tend to dissolve and in fact may not form at all. Local concentration gradients will determine the balance of dissolution and precipitation which are controlled by the mass transport to the bulk of the coolant (Lister *et al.*, 2001).

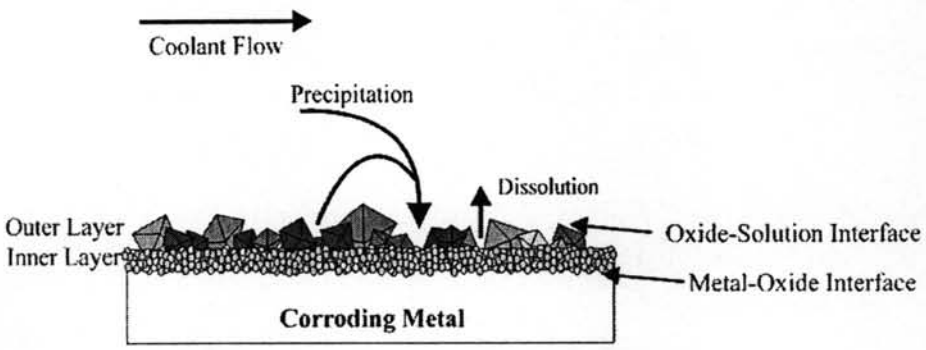

Figure 2.12 Schematic of carbon steel corroding in coolant under-saturated in dissolved iron (Lister *et al.*, 2001).

There are several proposed mechanisms for the formation of magnetite on carbon steel surface exposed to high temperature water.

Lang *et al.* (2002) considered the magnetite formation reaction as:

1) Most (about 88 %) of the hydrogen is probably generated at the M-O interface as iron goes into solution:

$$Fe + 2H_2O \longrightarrow Fe^{2+} + 2OH^- + H_2 \quad (2.5)$$

2) About one half of the ferrous species precipitate takes up the volume of the metal corroded:

$$3Fe^{2+} + 6OH^- \longrightarrow Fe_3O_4 + 2H_2O + H_2 \quad (2.6)$$

The magnetite is formed via the overall reaction scheme, a combination of reaction (1) and (2):

$$3Fe + 4H_2O \longrightarrow Fe_3O_4 + 4H_2 \quad (2.7)$$

Cook *et al.* (2004) has postulated the formation of magnetite as:

Step 1: $Fe \longrightarrow Fe^{2+} + 2e^-$ (2.8)

Step 2: $Fe^{2+} + 2H_2O \longrightarrow Fe(OH)_{2(aq)} + 2H^+$ (2.9)

Step 3: $Fe(OH)_{2(aq)} \longrightarrow Fe(OH)_{2(s)}$ (2.10)

Step 4: $3Fe(OH)_{2(s)} \longrightarrow Fe_3O_4 + 2\,H_2O + 2H^+ + 2e^-$ (2.11)

The overall reaction: $3Fe + 4H_2O \longrightarrow Fe_3O_4 + 4H_2$ (2.12)

The corrosion mechanisms coupled with the experimental information from operating reactors have formed the basis of a mechanistic model that describes carbon steel corrosion and predicts the oxide thickness with time in conditions conductive to FAC.